X-Ray Image Segmentation of the Hip Joint

Segmentation of the hip joint space based on a radial projection originating from the center of the femoral head

Kees Blok[1]

Supervisors: Jesse Krijthe[1]**, Gijs van Tulder**[1] **and Myrthe van den Berg**[1,2]

[1]**Electrical Engineering, Mathematics and Computer Science, Delft University of Technology, The Netherlands**
[2]**Orthopedics and Sports Medicine, Erasmus Medical Center, The Netherlands**

A Thesis Submitted to EEMCS Faculty Delft University of Technology,
In Partial Fulfilment of the Requirements
For the Bachelor of Computer Science and Engineering
June 22, 2024

Name of the student: Kees Blok
Final project course: CSE3000 Research Project
Thesis committee: Jesse Krijthe, Gijs van Tulder, Myrthe van den Berg, Xucong Zhang

Abstract

The severity of hip osteoarthritis is measured a.o. by the minimal distance between the femoral head and the acetabular roof in an X-ray image. However, the whole joint space profile might be a more accurate estimator, since it would include irregularities in the bone surface. These irregular bulges (osteophytes) on the bone surface are one of the signals that a person might have OA. Thus the stage of OA might be better estimated automatically by having this data in the joint space profile instead of just using the minimal joint space.

For this joint space profile, the distance between the femoral head and the acetabular roof needs to be calculated. Therefore, the positions of these parts in the hip joint are required to be know. These can be retrieved from e.g. a segmentation mask.

One way of calculating the distance in a joint is to use a radial projection. A radial projection is a way of projecting points from a curved space to a plane by projecting lines from a central point along increasing angles.

In this paper, we investigate how the joint space profile can be segmented most accurately from a radial projection originating from the center of the femoral head by several comparing noise filtering and edge-finding algorithms. After which is shown that a custom algorithm based on the theory behind edge detection in noisy images works most reliably and accurately.

There are still multiple points of improvement for this algorithm. The femoral head can be segmented more accurately than the acetabular roof, the segmentation of the latter could be optimized by detecting the brightest line (peaks) instead of the most sudden change (steepest gradient) in the X-ray image as the edge for the femoral head. The algorithm could be further improved by taking care of local outliers off those edges.

In conclusion, this paper compares multiple ways of segmenting the joint space of the hip joint. The best-performing algorithm could in the future be used in an assisting tool for doctors to highlight important irregularities and measurements in the hip joint space.

1 Introduction

Osteoarthritis (OA) is a growing health problem. In 2021, 1.589.600 people were estimated to have OA in the Netherlands. Of them, 28.700 people were newly diagnosed with OA in the hip joint (Vanhommerig, Poos, Gommer, Hendriks, & Giesbers, 2022). The diagnosis of OA is often based on metrics from X-ray images. The stage of OA can also be (partially) determined from those X-ray images. Such an X-ray image cropped to show the left hip joint can be seen in Figure 1.

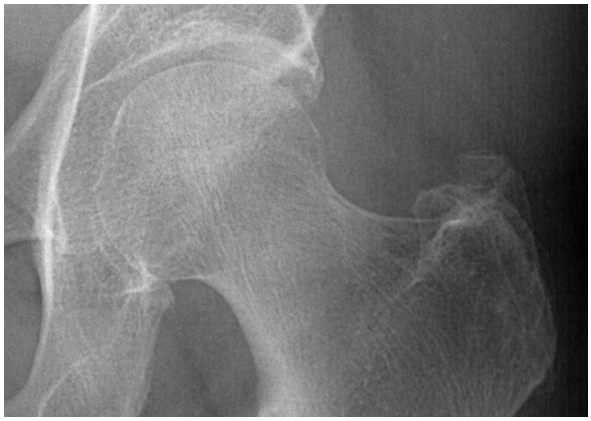

Figure 1: X-ray image of a left hip joint. Note that this X-ray image is taken from the front to the back of the person (anterior-posterior), which results in this hip showing on the right of the original image.

The most common feature used to determine the severity of hip OA from an X-ray image is the minimum joint space width, since this feature is associated most strongly with OA within X-ray images (Croft, Cooper, Wickham, & Coggon, 1990; Terjesen & Gunderson, 2012). The minimum joint space width is defined as the minimum distance between the two bones in the hip joint, namely the femoral head, the ball-shaped part of the femur (thighbone), and the acetabulum, the socket part of the hip.

This minimum joint space is used most often as one of the metrics to estimate the severity of OA, however, since it only focuses on the minimal distance, the severity of OA might be better estimated by the full joint space profile along the weight-bearing part of the acetabulum. Previous research has shown that multiple-joint space width (multiple distance measurements along the joint) is a better predictor for knee OA than minimal joint space width (Cheung, Tam, Chan, Chan, & Wen, 2021). Furthermore, the same research concluded that the highest number of points tested (64) along the joint performs the best. Therefore, the full joint space profile might be an even better estimator.

Since the hip joint is a ball-and-socket joint, a radial projection can be used to calculate the distance between the two parts in this joint more easily. A radial projection maps circular lines to straight lines. This works by projecting lines from a central point outwards. These lines are then put next to each other to create a rectangular shape. An example of a radial projection can be seen in Figure 2. The x-coordinates correspond to a certain angle, while the y-coordinates correspond to a certain distance from the center. In the radial projection, the distance between the two bone structures can be calculated as the vertical distance between the two lines.

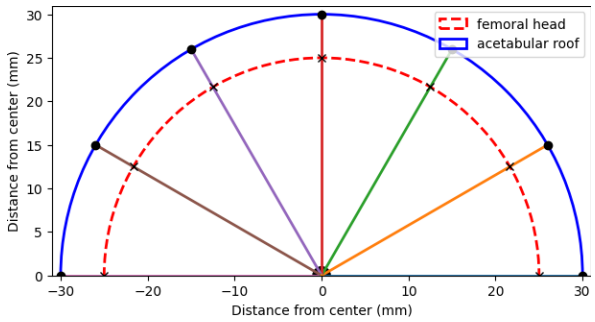

(a) Simplified hip joint

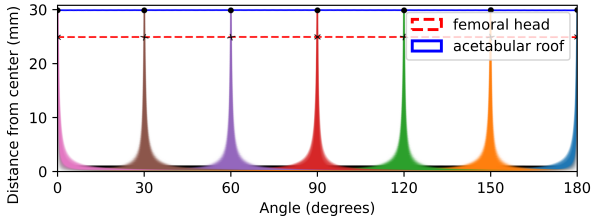

(b) Radial projection of the simplified hip joint

Figure 2: Example of a radial projection on a simplified hip joint. In (a) a simplified hip joint is shown. The red (dashed) line is the edge of the femoral head. The blue (continuous) line is the edge of the acetabular roof. In (b) the radial projection of (a) is shown.

The main advantage of using a radially projected image over a normal image is that no angles need to be calculated after the projection. This makes a big difference in the amount of computational power needed for, and the performance of certain edge-detection algorithms since most are naturally best at finding horizontal and/or vertical edges. The edges of the bone structures of interest should be approximately horizontal in this projected image.

In order to get an accurate joint space profile, an accurate segmentation of the joint space is needed, which can be obtained in several ways. Bone structures are often segmented with a (modified) UNet, a convolutional neural network (CNN) specifically developed for biomedical image segmentation (Ronneberger, Fischer, & Brox, 2015).

However, there are multiple disadvantages to using machine learning methods. CNNs need many annotated training samples to train, test, and validate to give a good result. Often, these CNNs are quite computationally intensive to run too (Ronneberger et al., 2015). Another disadvantage of many machine learning algorithms used for medical image segmentation is that they don't fully follow the ideal algorithm framework for healthcare (Loftus et al., 2022). This states that ideal algorithms for healthcare should be "explainable, dynamic, precise, autonomous, fair, and reproducible" (Loftus et al., 2022, para. 3). The main issue is that machine learning-based algorithms are often not explainable.

Another way to segment bone structures that follows this framework better in explainability is to use traditional edge-finding and segmentation algorithms. These don't need a large set of annotated samples for training. Only for the testing and validation of the accuracy, a test set of annotated samples is needed. Most importantly, these algorithms are explainable, which is a great advantage for medical applications, since it needs to be clear where measurements come from to make an informed decision. These algorithms are also autonomous and reproducible. Whether or not the other criteria for these ideal algorithms are met, depends on the implementation.

Therefore, in this paper, we investigate how the joint space profile can be segmented most accurately from a radial projection originating from the center of the femoral head by comparing multiple noise filtering and edge-finding algorithms.

This paper has the following structure: section 2 gives more information about the background of measuring the severity of OA and other related research. Next, section 3 explains the methods used in this research, after which the experimental setup is explained in section 4. The results of these experiments are shown in section 5. A reflection on some ethical aspects of this research is given in section 6, followed by the discussion in section 7. The paper ends with the conclusions and recommendations in section 8.

2 Related works

This section gives some background information on how X-ray images are used to measure the severity of OA in the hip after which some machine learning methods used in this field, their results, and limitations are mentioned.

2.1 Measuring the severity of OA from X-ray images

To score the severity of OA in the hip based on an X-ray image, often the Kellgren/Lawrence, Croft, or minimum joint space width metric is used (Kellgren & Lawrence, 1957; Croft et al., 1990; Terjesen & Gunderson, 2012). One of the features taken into account in the first two methods is the presence of irregular bulges (osteophytes) that sometimes grow on the surface of the bone when having OA (Terjesen & Gunderson, 2012). Another feature is the change in the shape of bones (Terjesen & Gunderson, 2012).

To get the minimum joint space width, the space between the femoral head and the acetabulum is often measured by hand from an X-ray image, which leads to inconsistent results. Since different doctors can interpret those images differently, their findings for the same patients can differ (Andersen et al., 2023). Furthermore, the same doctor interprets the same image also differently if they are shown the same image again after some time. This suggests that there is a need for a repeatable way of determining this minimum joint space width.

2.2 Machine learning methods

Therefore Andersen et al. (2023) researched whether it is possible to automate this procedure while giving more repeatable and consistent output. The proposed algorithm first crops to the region of interest for both hip joints. Then it segments the femoral and pelvic bones. Next, the contours of the top of the femoral head and the bottom of the acetabular sourcil (this is the densest line in the acetabular roof) are identified in this segmentation. Finally, it calculates the minimum Euclidean distance between these contours. Their segmentation algorithm consisted of a combination of deep learning and computer vision. Their results show that the automated method overestimates the minimum joint space width by 0.5 mm on average.

Other ways of segmenting the bone structures in the hip joint often include a (modified) U-Net for CT scans (Xu et al., 2022; Wu, Zhi, Liu, Zhang, & Chai, 2022). CT scans, however, have more information than a single X-ray image, since they consist of multiple images which together form a 3D view of the hip joint. These U-Net-based algorithms might need a lot of fine-tuning and post-processing to result in an accurate segmentation (Xu et al., 2022). Gebre et al. (2022) have shown that deep learning models on both a combination of CT scans and X-ray images and CT scans alone, result in a higher accuracy of detecting hip osteoarthritis.

3 Methodology

To be able to segment the joint space from a radial projection originating from the femoral head, this radial projection was needed first. After the radial projection, some preprocessing is done. Next, as much noise from the X-ray image as possible is removed with different algorithms to facilitate the segmentation process. Next, the segmentation using traditional edge-finding is explained. Also, a new edge-detection algorithm is introduced. Finally, some post-processing steps are explained which are necessary to help the doctors to interpret the data in the way they are used to.

3.1 Radial projection

Both methods use the radial projection originating from the center of the femoral head. A radial projection maps a Cartesian plane to a polar plane. For this projection, the center and radius of the femoral head are required. Using the same centers and radii, the X-ray image was cropped to the of interest (ROI) for the left and right hip joint separately. These cropped images then had the center of the femoral head in the middle of the bottom of the image and had a width and height proportional to the predicted radius (see Figure 2a). Next, a polar warping algorithm was used, which maps the cropped X-ray image to the radial projection originating from the center of the femoral head. A visual representation of the image cropped to the ROI and the radial projection of a simplified hip joint can be seen in Figure 2.

3.2 Preprocessing

The intensities of the image are clipped to the 10th and 100th percentile, after which they are normalized. This removes unnecessary information from the background while keeping as much information as possible from the rest of the image.

3.3 Removing noise

There are many different filters to remove noise from an image, however, most of these filters do not preserve the edges that are present in the image. These filters will remove valuable information which could otherwise be used to find the edges of the bones. Using these filters will thus probably result in a less accurate segmentation. So for this application, an edge-preserving filters sound to be more suitable.

However, due to how X-ray images are constructed (a ray either hits a certain point/pixel or not), the noise in the image is local and of a high relative amplitude. This has as effect that the gradient of this noise also has a high amplitude. Since edge-preserving filters use the gradient to determine if there is an edge, the noise is not filtered out well or not at all, since it is often also detected as edges.

In this paper, we compare one non-edge-preserving and multiple edge-preserving filters to evaluate which one works the best in this specific use case. These filters are chosen since they all have different approaches to removing noise in an image. The tested filters are:

- Gaussian blur
- Bilateral filter with a Gaussian spatial kernel (Tomasi & Manduchi, 1998)
- Bilateral filter with a flat spatial kernel
- Total variation denoising (Chambolle, 2004)
- Fast non-local means (Darbon, Cunha, Chan, Osher, & Jensen, 2008)
- Anisotropic diffusion (Perona & Malik, 1990)
- Difference of Gaussians (El-Sennary, Hussien, & Ali, 2019)

The first of these, Gaussian blur only blurs the image based on a Gaussian function and is not an edge-preserving filter, but is often used in image processing.

All the other filters are edge-preserving filters that work in different ways. The bilateral filter results in an image where the intensity of each pixel is the result of a weighted average of nearby pixels (Tomasi & Manduchi, 1998). Total variation denoising tries to reduce peaks in the input (Chambolle, 2004). This is done by solving a minimization problem which tries to find a signal with smaller gradients that is still close to the original signal. Fast non-local means finds similar patches in the image. Those patches are replaced with their average if they are close to each other.

Edges have a lower spatial frequency than noise. Gaussian filters with different sigmas filter out different frequencies. The difference between these filters results in a band-pass filter. This way, high-frequency noise can be filtered out, while edges can be kept. This idea is used in both Anisotropic diffusion and the difference of Gaussians. Difference of Gaussians uses just two Gaussian filters, while Anisotropic diffusion uses multiple.

3.4 Finding edges

Multiple edge-finding are tested to find out which one performs the best:

- Sobel operator
- Roberts cross
- Prewitt operator
- Canny edge detector
- Difference of Gaussians followed by a threshold
- Case-specific edge-finding algorithm

The first three of those edge-finding algorithms are differential operators. The idea for those three algorithms is that they approximate the gradient in the image. The gradient is calculated for each pixel in the x (G_x) and y (G_y) direction. These two gradients are combined using the formula $G = \sqrt{G_x^2 + G_y^2}$.

The Canny edge detector uses a more sophisticated multi-step method to reduce the number of false positives (Canny, 1986). First, it applies a Gaussian filter to the image to remove the high-frequency noise. Next, it uses an edge detection operator, often one of the three mentioned above, to find the gradient in the image. Next, it calculates the angle of the gradient for each pixel according to the formula $\theta = atan2(G_y, G_x)$. These angles are then rounded so that they fall in either of the 4 directions: horizontal, vertical, diagonal, and antidiagonal. The sign of the gradient represents in which direction the gradient goes up (for example left vs right for the horizontal direction). Next, it calculates if the gradient is larger (the sign does not matter here) in either the direction of the gradient or the opposite direction. This way, the strongest gradients along the edges are found, while the others are discarded.

Finally, these gradients are filtered based on their strength to remove low gradients which correspond to only small changes in the image and which are thus not considered to be edges. A threshold value is used to filter out all gradients that certainly belong to an edge ($G > T_{high}$). Next, all pixels directly next to one of these filtered pixels with a gradient larger than T_{low} (e.g. $G > T_{low}$), are considered to be part of an edge to. The idea behind this is that as many edges need to be included in the final image, while as much noise as possible needs to be excluded. So all edges where at least one pixel crosses the boundary T_{high} is considered an edge, while all others are removed.

Another algorithm is a difference of Gaussians followed by a threshold. The difference of Gaussians is a bandpass filter and can be used to filter out high-frequency noise and keep the edges. This filter subtracts an image with a large Gaussian blur from an image with a small Gaussian blur (El-Sennary et al., 2019). This results in an image without the high frequencies (noise) and the low frequencies (background or foreground), but which does include the frequencies in between, which should be the edges we are looking for. Next, all pixels with a value higher than a certain threshold will be seen as edges.

The last considered algorithm uses more background information on this specific use case. The idea is that the gradient only needs to be calculated in the y-direction in the radial projection since we are searching for an approximately horizontal line. By finding the largest peak and valley in this gradient close to where we expect them, we should be able to find where the intensities rise and drop the fastest, which should correspond to the location of the edge of the femoral head and acetabular roof respectively.

3.5 Creating a segmentation from the edges

The first five of these edge-finding algorithms will output multiple edges out of which, a segmentation needs to be made. Since the radius of the femoral head was already needed for the radial projection, it can be used here again. Since the edge of the femoral head should be the size of the radius apart from the center of the femoral head, this edge can be expected around where the y-coordinate equals the radius. The closest (continuous) edge can be filtered out to be the edge of the femoral head, while the first (continuous) edge above that one should be the edge of the acetabulum.

3.6 Postprocessing

To be able to interpret the segmentations better and to compare them to other segmentation methods, the segmentation needs to be brought back to the cartesian space. This is done by doing the inverse of the radial projection.

Another step of the postprocessing is to calculate a joint space profile from the radial segmentation. The joint space profile can for example be given as a list of distances. There each value represents the distance from the femoral head to the acetabulum and each index corresponds to an angle from the center of the femoral head. This distance can be calculated as the vertical distance between the edge of the femoral head and the acetabular roof, while the angle directly corresponds to the x-coordinate in the radial projection. (see Figure 2).

4 Experimental setup

In this section, the experimental setup will be explained in more detail. First, the used datasets will be discussed. Next, the ground truth for this experiment is introduced. After this, the implementation of the radial projection, noise-removing filters, and edge-finding algorithms are discussed.

4.1 Datasets

We use data from two public datasets. The first dataset is from the Cohort Hip and Cohort Knee (CHECK) study (Wesseling et al., 2016), which studied the development of (early) symptoms of OA in the hip and/or knee of 1002 participants who had the early symptoms of pain in their hip and/or knee. Those participants visited the research center for multiple years where the researchers took X-ray images and other measurements at each visit. The X-ray images of the hips of these participants are used in this study.

The Osteoarthritis Initiative (OAI) study (Eckstein, Kwoh, & Link, 2014) is another prospective study of OA of which the data is open-access. From this study, the X-ray images of the hip of multiple visits of 4755 participants were available for use in the development of the proposed algorithm.

4.2 Ground Truth

To be able to verify the accuracy of the detection of the edges of the bone structure from the proposed algorithm, a ground truth needed to be introduced. For this study, BoneFinder (Lindner, Thiagarajah, Wilkinson, Wallis, & Cootes, 2013) was used to generate the ground truth. BoneFinder is a fully automatic system that localizes specified landmark points in X-ray images.

4.3 Radial projection

The center and radius of the femoral head are required for the radial projection. These were calculated from a circle fitted (Taubin, 1991) to the BoneFinder points corresponding to the femoral head. These points are in the range [18, 27] for the right hip and [98, 107] for the left hip.
All steps following this line are executed for the left and right hip separately. The X-ray image is cropped to three times the radius of the corresponding hip in width and one-and-a-half times the radius in height. The center of the femoral head is then in the bottom center of the cropped image. Finally, the image is mapped to polar coordinate space, as can be seen in Figure 3.

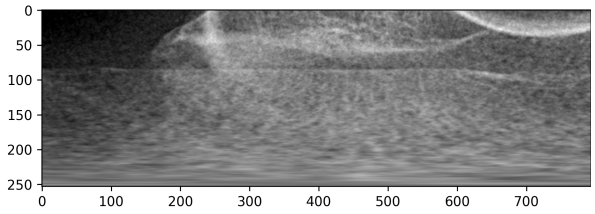

Figure 3: Radial projection of the top half of the hip joint

4.4 Removing noise

The mentioned (edge-preserving) filters are run with only some basic fine-tuning of the parameters since fully fine-tuning all parameters without overfitting to a small number of images would have taken too much time for this research.

4.5 Finding edges with standard edge-finding algorithms

The mentioned edge-finding algorithms are run with more fine-tuning on a small set of images.

For the difference of Gaussians filter with threshold, minimum cross entropy thresholding(Li & Tam, 1998) was used to get a threshold which is used to set everything below it to black and the rest of the image to white. Next, some small blobs are removed to remove even more noise. After these small blobs are removed, a contour-finding algorithm is used to find the edges of the remaining blobs.

The radius of the femoral head is already known as it is needed to crop to the correct region of interest. This radius is also used here as an estimation of where the edge of the bone of the femoral head should be. For each point on that line, the closest edge is stored, after which from these closest edges, a new line is constructed.

4.6 Custom edge-finding algorithm

The case-specific edge-finding algorithm uses more background information about this specific use case by only finding two edges in the image. First, it crops the image to a specific region in the radially projected image where it will approximate the location of the joint space. This region is in the x-direction the middle third, which corresponds to 60 degrees centered above the center of the femoral head in the Cartesian space. In the y-direction, this is from the top of the image to the radius of the femoral head (the same as used before to crop the hip joint out of the image) plus an extra 5 millimeters (converted to pixels). These extra 5 millimeters account for some error in this radius and allow for a more accurate calculation of the gradient around that point. An example of such a region of interest can be seen in Figure 4).

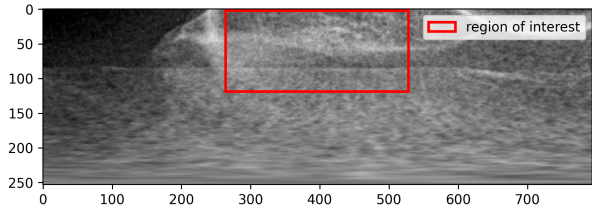

Figure 4: Region of interest for approximating the edge of the femoral head and acetabular roof

Next, the gradient along the x-axis is calculated with the intensities of the pixels within this ROI. First, the intensities of all pixels are averaged in the x-direction. Next, a moving average (window width of 7) is used to filter out small intensity changes in this mean. This is followed by the calculation of the slope and finally this is again followed by a moving average (window width of 5) to filter out small irregularities. An example of some plots of these lines can be seen in Figure 5.

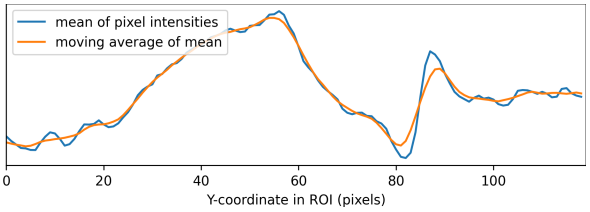

(a) Mean along x-axis

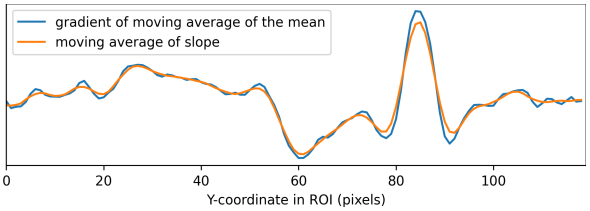

(b) Gradient of the mean

Figure 5: Example of the average of pixel intensities in the region of interest (ROI) along the x-axis, with its moving average (a). And the gradient of (the moving average of) the mean and its moving average (b).

Finally, the average edge of the femoral head and the acetabular roof are calculated. The average edge of the femoral head is determined to be at the top of the peak closest to the aforementioned radius (in the example plot Y=85). We know that the edge of the acetabular roof should be above the edge of the femoral head. Therefore we only look at the range above the found edge of the femoral head. The average edge of the acetabular roof is determined to be at the bottom of the valley with the largest prominence in this range (in the example plot Y=61). The prominence indicates how much the peak (or valley in this case) stands out from others. This is measured by the difference in height between the peak and its baseline (where the slope first crosses 0).

Next, the same method of finding the largest prominences is used on each column in the image to determine the peaks and valleys in the gradient. Using the average edges calculated before, the peaks and valleys that are most likely to correspond to the actual edges are found by calculating the formula $prominence/(abs(distance\_from\_expected\_line) + 1)$ for each peak and valley and picking the largest of those as the final edge.

Next, a moving average is used to smoothen out some of the peaks that occurred due to the absence of the high gradient at the correct place in the image, since this is done pixel-by-pixel in the x-direction.

Finally, the same average edge method is used in the other direction (average of the Y-axis), to find the starting point of the femoral head. All the values of (moving average of) the edge of the femoral head before that are set to 0.

5 Results

Multiple algorithms for removing the noise and finding edges are tested, of which only the custom edge-finding algorithm was able to segment the joint space in some way for every given image.

5.1 Difference of Gaussians with thresholding

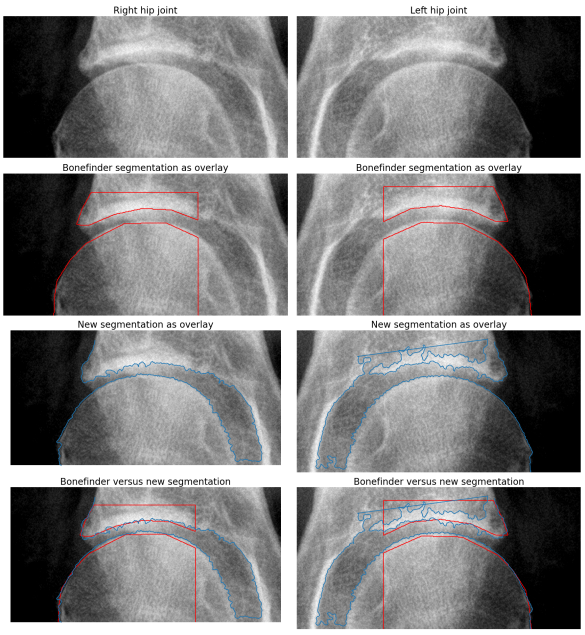

Figure 6: Example of the BoneFinder segmentation and the segmentation using the difference of Gaussians on two hips.

The difference of Gaussians followed by a thresholding algorithm showed some promising results for some images. An example of the resulting segmentation in such an image can be seen in Figure 6. However, for other images, half of the edges were removed due to the step that removes small blobs, which results in no joint space segmentation. An example of this can be seen in Figure 7.

5.2 Custom edge-finding algorithm

The custom edge-finding algorithm gives the best results since it always gives a line for both the femoral head and the acetabular roof. An example of the results of this algorithm is shown in Figure 8a.

This algorithm sometimes incorrectly identifies the end of the acetabular roof (see the right side left hip joint in Figure 8a). This is a result of the way how this end position is calculated. In the cases where the end is incorrectly identified, the intensity difference is not the largest at the end of the femoral head, but just before or after it where another part of the pelvis ends.

5.3 Other tested algorithms

Some of the other results are shown in Figure 9. Not all tested combinations are shown due to the amount combinations of

different algorithms and parameters.

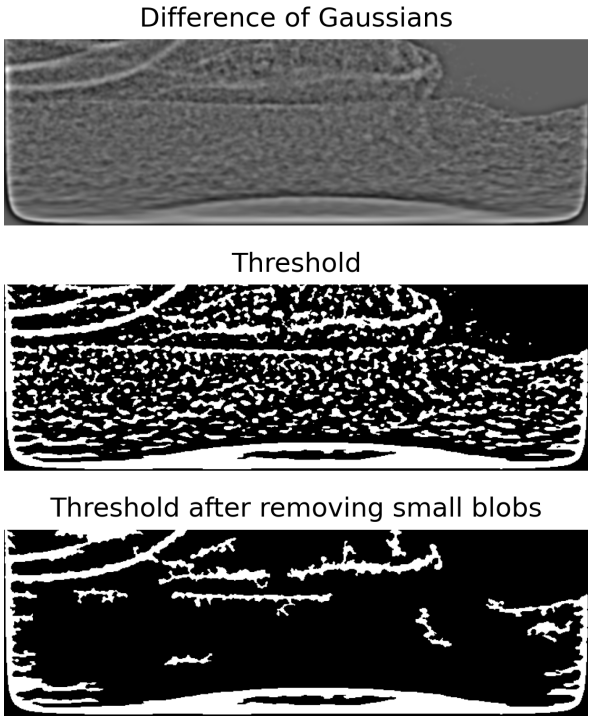

Figure 7: Example of image with the correct edges due to too many small blobs being removed.

6 Responsible Research

In this research non-machine learning methods have been used to see if they can accurately segment the joint space in the hip joint from an X-ray image.

Machine learning algorithms like those discussed in section 2, need to train on large datasets for extended periods of time. This results in the need for powerful computers and possibly GPUs to speed up the computation. Those use a large amount of electrical power to train and test their models. The electricity in the Netherlands still comes for more than 50 percent from fossil fuels (Netherlands, 2024), which is an ending source of power. Furthermore, the burning of those fossil fuels brings large amounts of CO2 into the air, which indirectly leads to global warming.

Furthermore, this research tries to help doctors to make the assessment of OA from X-rays easier, by providing an automated method to calculate the joint space profile, thus relieving the healthcare industry from some work.

Finally, because of this method, patients might get a more suitable treatment for hip OA, since this automated method is fully consistent between readings, which doctors are not.

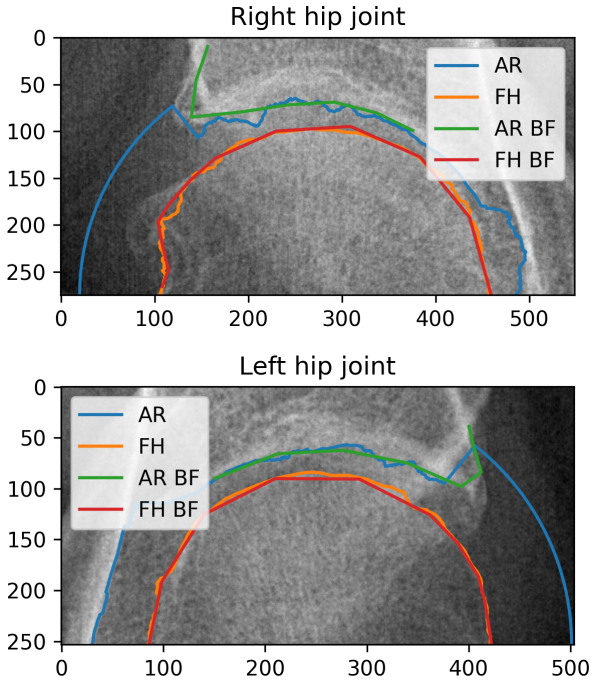

(a) Example of the custom edge-finding algorithm compared to BoneFinder. ”AR” = acetabular roof, ”FH” = femoral head, ”BF” = BoneFinder

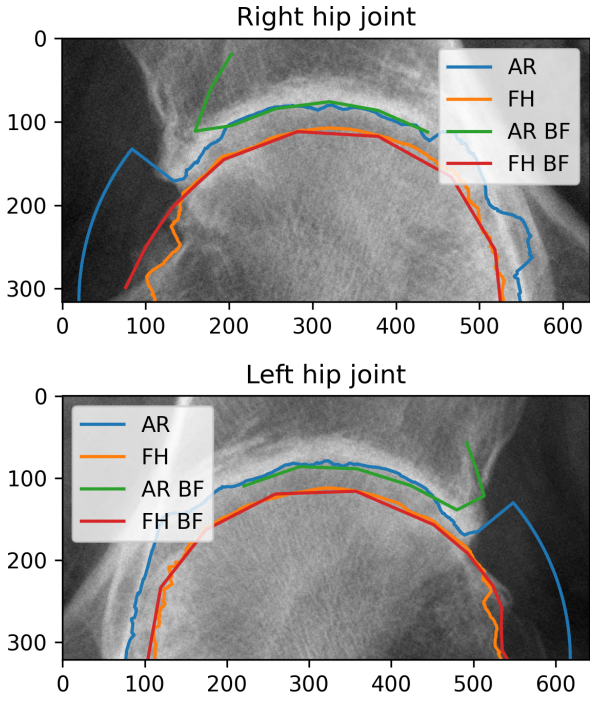

(b) Example of the custom edge-finding algorithm compared to BoneFinder where BoneFinder incorrectly annotated the end of the acetabular roof. ”AR” = acetabular roof, ”FH” = femoral head, ”BF” = BoneFinder

Figure 8: Custom edge-finding algorithm compared to BoneFinder

7 Discussion

This research aimed to accurately segment the joint space from a radial projection originating from the center of the femoral head using edge-finding and segmentation algorithms.

The difference of Gaussians with thresholding will need some improvements like selectively removing small blobs from the thresholded image to work reliable enough to always give a valid segmentation.

The custom edge-finding algorithm might need some improvements too, like a different way of finding the end of the acetabular roof, before this method can actually be used.

It is not always clear whether the edge is determined correctly at the acetabular roof (for example in Figure 6. The identified edge is not as smooth of a curve as the one of the femoral head. Therefore a professional was asked to determine how the edge should look like in this case. This professional mentioned that the bone of the acetabular roof most likely has some more dense spots. This can be seen in the image as a lighter spot when compared to the surroundings. The algorithm used for locating this line looks for edges, which are changes in the intensity of the image. Thus the edge-finding algorithm sees these more dense spots which are close to the actual edge (incorrectly) as the edge itself.

The output of BoneFinder, which is used as ground truth, is in a format different from the output of the proposed algorithm, which makes the comparison less reliable. BoneFinder outputs only a specified number of points. This means that the lines generated from the BoneFinder points can not have the same level of detail as the proposed algorithm. Therefore, the comparison is not fair when looking at a low level of detail, since BoneFinder is missing it.

This suggest that the should be a ground truth with a higher level of detail to determine the accuracy of the proposed algorithm. However, there is no such a reliable and accurate automatic segmentation algorithm for hip joints yet. Therefore this research was done to try to find a new and better segmentation algorithm.

8 Conclusion and recommendations

This aim of this paper was to find out if and how the joint space be segmented most accurately from a radial projection originating from the center of the femoral head using edge-finding?

First is seen how the images are transformed with a radial projection from the center of the femoral head, after which they are preprocessed by rescaling the intensity.

Next, it was found that a difference of Gaussians can be used as an edge-preserving filter in this specific use-case and that a custom edge-finding algorithm works even better.

It would be of interest how the segmentation would perform without the radial projection since that part of the algorithm might introduce additional (computational) complexity without increasing the accuracy of the final segmentation.

Currently, the center and radius of the femoral head are calculated from the BoneFinder output, since finding them is not the main point of this research. In the future, this could be done by a convolutional neural network (CNN) trained to output the center (x and y coordinates) and the radius of the femoral head using a circle fitted to the Bonefinder output.

So in conclusion, this paper shows an alternative way to segment the joint space using traditional image segmentation and edge-finding algorithms.

This algorithm can be used to calculate a full joint space profile, which might be able to give more information about the stage of hip OA than the often currently used minimal joint space width. This would result in a better way of assisting doctors with automatically determining the stage of OA.

References

Andersen, A. M., Rasmussen, B. S. B., Graumann, O., Overgaard, S., Lundemann, M., Haubro, M. H., … Jensen, J. (2023, September). Minimal Hip Joint Space Width Measured on X-rays by an Artificial Intelligence Algorithm—A Study of Reliability and Agreement. *BioMedInformatics*, *3*(3), 714–723. Retrieved 2024-04-22, from `https://www.mdpi.com/2673-7426/3/3/46` (Number: 3 Publisher: Multidisciplinary Digital Publishing Institute) doi: 10.3390/biomedinformatics3030046

Canny, J. (1986, December). A Computational Approach To Edge Detection. *Pattern Analysis and Machine Intelligence, IEEE Transactions on*, *PAMI-8*, 679–698. doi: 10.1109/TPAMI.1986.4767851

Chambolle, A. (2004, January). An Algorithm for Total Variation Minimization and Applications. *Journal of Mathematical Imaging and Vision*, *20*(1), 89–97. Retrieved 2024-06-22, from `https://doi.org/10.1023/B:JMIV.0000011325.36760.1e` doi: 10.1023/B:JMIV.0000011325.36760.1e

Cheung, J. C.-W., Tam, A. Y.-C., Chan, L.-C., Chan, P.-K., & Wen, C. (2021, October). Superiority of Multiple-Joint Space Width over Minimum-Joint Space Width Approach in the Machine Learning for Radiographic Severity and Knee Osteoarthritis Progression. *Biology*, *10*(11), 1107. doi: 10.3390/biology10111107

Croft, P., Cooper, C., Wickham, C., & Coggon, D. (1990, September). Defining osteoarthritis of the hip for epidemiologic studies. *American Journal of Epidemiology*, *132*(3), 514–522. doi: 10.1093/oxfordjournals.aje.a115687

Darbon, J., Cunha, A., Chan, T. F., Osher, S., & Jensen, G. J. (2008, May). Fast nonlocal filtering applied to electron cryomicroscopy. In *2008 5th IEEE Interna-*

tional Symposium on Biomedical Imaging: From Nano to Macro (pp. 1331–1334). Retrieved 2024-06-10, from https://ieeexplore.ieee.org/document/4541250 (ISSN: 1945-8452) doi: 10.1109/ISBI.2008.4541250

Eckstein, F., Kwoh, C., & Link, T. (2014, April). Imaging research results from the Osteoarthritis Initiative (OAI): A review and lessons learned 10 years after start of enrolment. *Annals of the rheumatic diseases*, *73*. doi: 10.1136/annrheumdis-2014-205310

El-Sennary, H. A. E.-F., Hussien, M. E., & Ali, A. E.-M. A. (2019, December). Edge Detection of an Image Based on Extended Difference of Gaussian. *American Journal of Computer Science and Technology*, *9*(1), 35–47. Retrieved 2024-06-10, from http://www.sciencepg.com/article/10.11648/j.ajcst.20190203.11 (Number: 1 Publisher: Science Publishing Group) doi: 10.11648/j.ajcst.20190203.11

Kellgren, J. H., & Lawrence, J. S. (1957, December). Radiological assessment of osteo-arthrosis. *Annals of the Rheumatic Diseases*, *16*(4), 494–502. doi: 10.1136/ard.16.4.494

Li, C. H., & Tam, P. K. S. (1998, June). An iterative algorithm for minimum cross entropy thresholding. *Pattern Recognition Letters*, *19*(8), 771–776. Retrieved 2024-06-03, from https://www.sciencedirect.com/science/article/pii/S0167865598000579 doi: 10.1016/S0167-8655(98)00057-9

Lindner, C., Thiagarajah, S., Wilkinson, J. M., Wallis, G. A., & Cootes, T. F. (2013). Fully automatic segmentation of the proximal femur using random forest regression voting. *IEEE Transactions on Medical Imaging*, *32*(8), 1462–1472. Retrieved 2024-06-10, from https://research.manchester.ac.uk/en/publications/fully-automatic-segmentation-of-the-proximal-femur-using-random-f (Publisher: IEEE) doi: 10.1109/TMI.2013.2258030

Loftus, T. J., Tighe, P. J., Ozrazgat-Baslanti, T., Davis, J. P., Ruppert, M. M., Ren, Y., … Bihorac, A. (2022, January). Ideal algorithms in healthcare: Explainable, dynamic, precise, autonomous, fair, and reproducible. *PLOS Digital Health*, *1*(1), e0000006. Retrieved 2024-06-21, from https://journals.plos.org/digitalhealth/article?id=10.1371/journal.pdig.0000006 (Publisher: Public Library of Science) doi: 10.1371/journal.pdig.0000006

Netherlands, S. (2024, March). *Nearly half the electricity produced in the Netherlands is now renewable* [webpagina]. Retrieved 2024-06-22, from https://www.cbs.nl/en-gb/news/2024/10/nearly-half-the-electricity-produced-in-the-netherlands-is-now-renewable (Last Modified: 2024-03-07T15:00:00+01:00) doi: 10/nearly-half-the-electricity-produced-in-the-netherlands-is-now-renewable

Perona, P., & Malik, J. (1990, July). Scale-space and edge detection using anisotropic diffusion. *IEEE Transactions on Pattern Analysis and Machine Intelligence*, *12*(7), 629–639. Retrieved 2024-06-10, from https://ieeexplore.ieee.org/document/56205 (Conference Name: IEEE Transactions on Pattern Analysis and Machine Intelligence) doi: 10.1109/34.56205

Ronneberger, O., Fischer, P., & Brox, T. (2015, May). *U-Net: Convolutional Networks for Biomedical Image Segmentation.* arXiv. Retrieved 2024-06-21, from http://arxiv.org/abs/1505.04597 (arXiv:1505.04597 [cs]) doi: 10.48550/arXiv.1505.04597

Taubin, G. (1991, December). Estimation of Planar Curves, Surfaces, and Nonplanar Space Curves Defined by Implicit Equations with Applications to Edge and Range Image Segmentation. *Pattern Analysis and Machine Intelligence, IEEE Transactions on*, *13*, 1115–1138. doi: 10.1109/34.103273

Terjesen, T., & Gunderson, R. B. (2012, April). Radiographic evaluation of osteoarthritis of the hip. *Acta Orthopaedica*, *83*(2), 185–189. Retrieved 2024-04-27, from https://www.ncbi.nlm.nih.gov/pmc/articles/PMC3339535/ doi: 10.3109/17453674.2012.665331

Tomasi, C., & Manduchi, R. (1998, January). Bilateral filtering for gray and color images. In *Sixth International Conference on Computer Vision (IEEE Cat. No.98CH36271)* (pp. 839–846). Retrieved 2024-06-10, from https://ieeexplore.ieee.org/document/710815 doi: 10.1109/ICCV.1998.710815

Vanhommerig, J., Poos, M., Gommer, A., Hendriks, C., & Giesbers, H. (2022, November). *Artrose | Leeftijd en geslacht | Volksgezondheid en Zorg*. Retrieved 2024-04-22, from https://www.vzinfo.nl/artrose/leeftijd-en-geslacht

Wesseling, J., Boers, M., Viergever, M. A., Hilberdink, W. K., Lafeber, F. P., Dekker, J., & Bijlsma, J. W. (2016, February). Cohort Profile: Cohort Hip and Cohort Knee (CHECK) study. *International Journal of Epidemiology*, *45*(1), 36–44. Retrieved 2024-06-03, from https://academic.oup.com/ije/article-lookup/doi/10.1093/ije/dyu177 doi: 10.1093/ije/dyu177

Wu, D., Zhi, X., Liu, X., Zhang, Y., & Chai, W. (2022, March). Utility of a novel integrated deep convolutional neural network for the segmentation of hip joint from computed tomography images in the preoperative planning of total hip arthroplasty. *Journal of Orthopaedic Surgery and Research*, *17*, 164. Retrieved 2024-06-22, from https://www.ncbi.nlm.nih.gov/pmc/articles/PMC8922800/ doi: 10.1186/s13018-022-02932-w

Xu, P., Moshfeghifar, F., Gholamalizadeh, T., Nielsen, M. B., Erleben, K., & Darkner, S. (2022). *Auto-segmentation of Hip Joints using MultiPlanar UNet with Transfer learning*. doi: 10.48550/arXiv.2208.08226

Appendix

Figure 9: A grid of the output of different algorithms, where each column has a different input image, which is shown in the first row.